

Loss of *GLIS2* causes nephronophthisis in humans and mice by increased apoptosis and fibrosis

Massimo Attanasio^{1,8}, N Henriette Uhlenhaut^{2,8}, Vitor H Sousa^{2,7}, John F O'Toole¹, Edgar Otto¹, Katrin Anlag², Claudia Klugmann², Anna-Corina Treier², Juliana Helou¹, John A Sayer¹, Dominik Seelow^{3,4}, Gudrun Nürnberg^{3,4}, Christian Becker^{3,4}, Albert E Chudley⁵, Peter Nürnberg^{3,6}, Friedhelm Hildebrandt¹ & Mathias Treier²

Nephronophthisis (NPHP), an autosomal recessive kidney disease, is the most frequent genetic cause of end-stage renal failure in the first three decades of life. Positional cloning of the six known NPHP genes^{1–4} has linked its pathogenesis to primary cilia function^{3,5}. Here we identify mutation of *GLIS2* as causing an NPHP-like phenotype in humans and mice, using positional cloning and mouse transgenics, respectively. Kidneys of *Glis2* mutant mice show severe renal atrophy and fibrosis starting at 8 weeks of age. Differential gene expression studies on *Glis2* mutant kidneys demonstrate that genes promoting epithelial-to-mesenchymal transition and fibrosis are upregulated in the absence of *Glis2*. Thus, we identify *Glis2* as a transcription factor mutated in NPHP and demonstrate its essential role for the maintenance of renal tissue architecture through prevention of apoptosis and fibrosis.

The group of recessive kidney diseases represented by NPHP shares pathogenic features with other cystic kidney diseases³ but differs in that kidney enlargement is absent and fibrosis is predominant⁶. Positional cloning of genes mutated in NPHP has been instrumental for generating a unifying pathogenic theory of cystic kidney diseases^{3,7}. Although hyperproliferation has been demonstrated in polycystic kidney disease, no data exist on the mechanisms of progressive reduction of kidney size in nephronophthisis. In this manuscript, we provide data on enhanced apoptosis and fibrosis in a newly generated

mouse model of nephronophthisis. All known variants of NPHP have in common the characteristic renal histological pattern of diffuse interstitial cell infiltration with fibrosis, tubular basement membrane disintegration with tubular atrophy and, in some instances, cyst formation, which progressively leads to end stage kidney disease (ESKD) at a median age of 13 years⁶. As mutations in the six known NPHP genes (*NPHP1*, *INVS* (*NPHP2*), *NPHP3*, *NPHP4*, *ICQBI* (*NPHP5*) and *CEP290* (*NPHP6*))^{1–4} are found in only 35% of cases with nephronophthisis³, and as its molecular pathogenesis remains elusive, we sought additional causative genes by positional cloning. Therefore, we performed a genome-wide search for linkage in

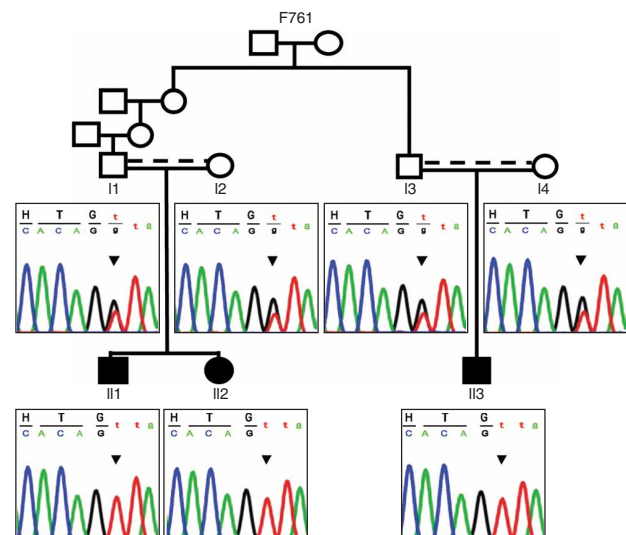


Figure 1 Haplotype analysis at the *GLIS2* locus on chromosome 16p in the consanguineous kindred F761. Circles represent females; squares represent males. Filled symbols correspond to individuals with NPHP. Arrowheads in the chromatograms indicate the mutation (IVS5+1G>T) at the first base of intron 5 that abrogates the obligatory splice site. The mutation is homozygous in all affected children and heterozygous in all four parents.

¹Departments of Pediatrics and of Human Genetics, University of Michigan, Ann Arbor, Michigan 48109, USA. ²Developmental Biology Unit, European Molecular Biology Laboratory, D-69117 Heidelberg, Germany. ³Cologne Center for Genomics, University of Cologne, D-50674 Cologne, Germany. ⁴RZPD Deutsches Ressourcenzentrum für Genomforschung GmbH, D-14059 Berlin, Germany. ⁵Departments of Pediatrics and Child Health, Biochemistry and Medical Genetics, University of Manitoba, Winnipeg, Manitoba R3E3P4, Canada. ⁶Institute for Genetics, University of Cologne, D-50674 Cologne, Germany. ⁷Present address: Smilow Research Center, New York University, New York, New York 10016, USA. ⁸These authors contributed equally to this work. Correspondence should be addressed to F.H. (fhilde@med.umich.edu) or M.T. (treier@embl.de).

Received 27 November 2006; accepted 17 May 2007; published online 8 July 2007; doi:10.1038/ng2072

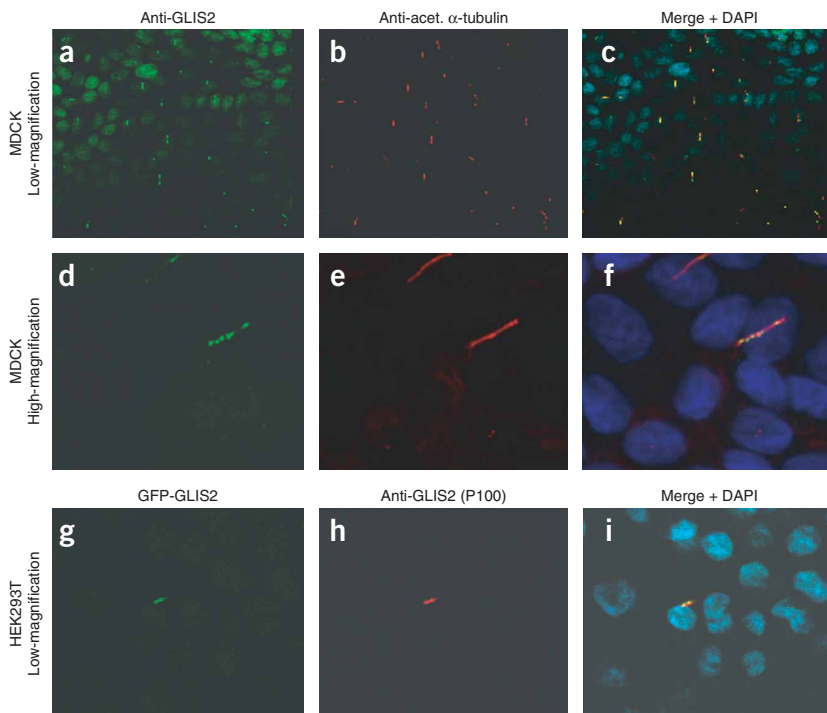


Figure 2 GLIS2 localizes to both nuclei and primary cilia in renal epithelial cell cultures. (a–f) Confluent MDCK-II cells were examined by immunofluorescence using primary antibodies to GLIS2 (P100) (green) and acetylated α -tubulin (red). DAPI nuclear staining is shown in blue. Images were taken at low (a–c) and high (d–f) magnification. Note that GLIS2 colocalizes to primary cilia with acetylated α -tubulin and is partially detectable in the nucleus (a,d,c,f). At higher electronic magnification (3 \times) (d–f) of two ciliary structures, GLIS2 localizes in a punctate pattern along the ciliary axoneme. (g–i) To confirm the specificity of P100 for GLIS2, HEK293T cells were transfected with an N-terminal GFP-tagged full-length construct of GLIS2 (green autofluorescence) and were incubated with P100 (red). Overexpressed GFP-tagged GLIS2 colocalizes with P100 (i), demonstrating antibody specificity.

three individuals developed ESKD by 8 years of age and underwent renal transplantation. Kidney histology of all three affected individuals was consistent with the diagnosis of NPHP. A genome-wide profile of nonparametric LOD scores (NPL) in this kindred yielded nine regions of homozygosity represented by peaks with NPL > 4 (Supplementary Fig. 1 online). When genotyping highly informative microsatellite markers in these regions, the peak on human chromosome 16p was confirmed for potential homozygosity by descent, thereby defining a putative locus (NPHP7)

25 consanguineous kindred using the GeneChip Human Mapping 10K microarray from Affymetrix. Of the 25 pedigrees studied, a Canadian Oji-Cree kindred (F761) with a high grade of consanguinity had two siblings and a third-degree cousin with NPHP. All

represented by peaks with NPL > 4 (Supplementary Fig. 1 online). When genotyping highly informative microsatellite markers in these regions, the peak on human chromosome 16p was confirmed for potential homozygosity by descent, thereby defining a putative locus (NPHP7)

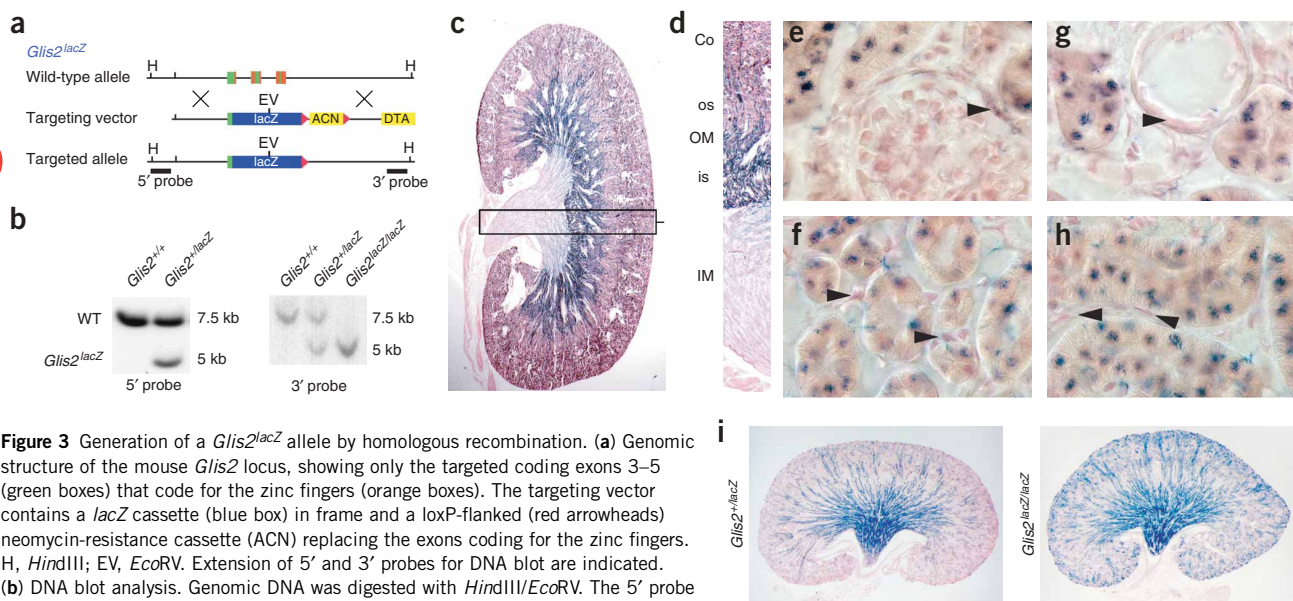


Figure 3 Generation of a *Glis2^{lacZ}* allele by homologous recombination. (a) Genomic structure of the mouse *Glis2* locus, showing only the targeted coding exons 3–5 (green boxes) that code for the zinc fingers (orange boxes). The targeting vector contains a *lacZ* cassette (blue box) in frame and a loxP-flanked (red arrowheads) neomycin-resistance cassette (ACN) replacing the exons coding for the zinc fingers. H, *HindIII*; EV, *EcoRV*. Extension of 5' and 3' probes for DNA blot are indicated. (b) DNA blot analysis. Genomic DNA was digested with *HindIII/EcoRV*. The 5' probe detected the expected 7.5-kb wild-type band and the 5-kb mutant band, whereas the 3' probe detected the 7.5-kb wild-type band and a 5-kb mutant band after removal of the selection cassette. (c) β -galactosidase staining of an 8-week-old adult *Glis2^{lacZ/+}* heterozygous kidney showing *lacZ* expression in cells of all renal tubule segments with enhancement in the corticomedullary junction. (d) Magnification of c, showing cortex (Co), outer medulla (OM; os, outer stripe; is, inner stripe) and inner medulla (IM). (e–h) Magnification of d, demonstrating expression of *Glis2* throughout all renal tubule segments and epithelial cells of Bowman's capsule (arrowhead in e) but not in glomerular (e), mesenchymal (arrowheads in f,h) or endothelial cells (arrowhead in g). (i) β -galactosidase staining of 5-d-old kidneys from heterozygous *Glis2^{lacZ/+}* (left) and homozygous (right) *Glis2^{lacZ/lacZ}* mice, showing no obvious difference in histological appearance between the two genotypes. Increased β -galactosidase staining in *Glis2^{lacZ/lacZ}* mutant kidneys is due to two *lacZ* copies.

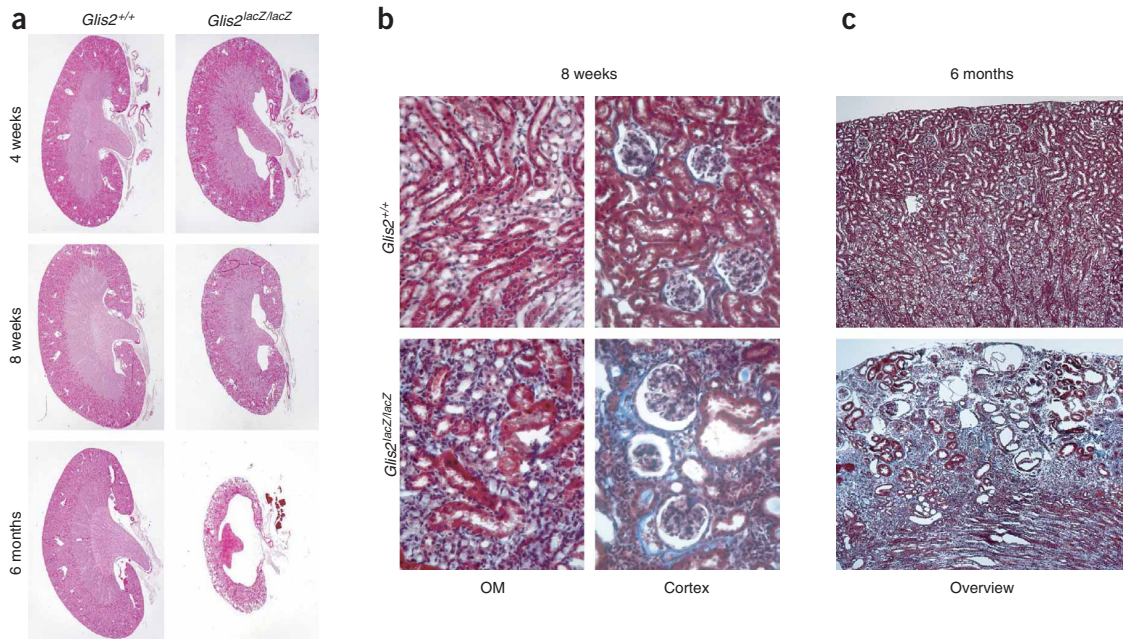


Figure 4 Time course of renal degeneration in *Glis2^{lacZ/lacZ}* mutant mice. **(a)** PAS staining of wild-type and *Glis2^{lacZ/lacZ}* mutant kidneys at different time points. Whole kidney sections from 4-week-old, 8-week-old and 6-month-old wild-type and *Glis2^{lacZ/lacZ}* mutant mice are shown. All images were taken at the same magnification. *Glis2^{lacZ/lacZ}* mutant kidneys become smaller in size over time, mainly owing to a reduction in size of the medulla region. Note that loss of corticomedullary differentiation, a characteristic hallmark of NPHP, is appreciable at 4 weeks and pronounced at 8 weeks. **(b,c)** Trichrome-Masson staining of 8-week-old and 6-month-old wild-type and *Glis2^{lacZ/lacZ}* mutant kidneys. **b** shows transverse sections of the outer medulla (OM) region and sagittal sections of the cortical region, which show collagen deposition and diffuse tubulointerstitial cell infiltration in *Glis2^{lacZ/lacZ}* mutant kidneys. **c** shows a sagittal overview of the outer medulla and cortical region of 6-month-old kidneys, demonstrating the characteristic phenotypic changes of NPHP in *Glis2^{lacZ/lacZ}* mutant kidneys.

for nephrophtosis type 7. The interval of homozygosity between the two flanking heterozygous markers *D16S475* and *SNP_A-1509814* spanned 2.5 Mb and was further confirmed when typing three additional polymorphic microsatellites.

This region included the *GLIS2* gene, which encodes a Kruppel-like zinc finger transcription factor⁸. *Glis2* is most abundantly expressed in adult mouse kidney and, during metanephric development, in the ureteric bud, the inducer of mesenchymal-to-epithelial conversion during nephron tubule formation⁹. Direct sequencing of the six *GLIS2* coding exons uncovered a homozygous transversion IVS5+1G>T in all three affected individuals. This abrogates the 5' obligatory splice donor site of exon 5 and is predicted to result in a nonfunctional protein. The mutation segregates in all affected family members consistently with an autosomal recessive disease (Fig. 1). We further corroborated the pathogenic role of this mutation by demonstrating its absence from 94 healthy control individuals. As it was not possible to obtain RNA from the affected individuals in family F761, we used a minigene construct demonstrating that the IVS5+1G>T mutation does, in fact, interfere with splicing (Supplementary Fig. 2 and Supplementary Methods online). When we screened a worldwide cohort of 470 individuals with NPHP-like phenotypes, no additional mutations were detected. We thereby identified a mutation of *GLIS2* as a new cause of NPHP (NPHP type 7). NPHP7 is a very rare cause of NPHP, similar to the situation seen in the *INVS* (inversin, also known as *NPHP2*) mutation².

Five of six NPHP proteins (nephrocystins) identified so far have been shown to be expressed in primary cilia or basal bodies of renal epithelial cells^{2,4,10}, a finding that was central to the generation of a

unifying pathogenic theory of cystic kidney disease as 'ciliopathies'^{3,5}. To test whether this paradigm would be valid for *GLIS2* as well, we examined *GLIS2* expression in the renal epithelial cell line MDCK-II by coimmunolocalization with acetylated α -tubulin by confocal laser microscopy using the P100 antibody to *GLIS2* (anti-*GLIS2*). We demonstrate that *GLIS2* is expressed in MDCK-II cells along the ciliary axoneme in a punctate pattern similar to the pattern seen for other nephrocystins^{2,4,10} (Fig. 2a-f), thereby confirming ciliary expression also for *GLIS2*. We demonstrated the specificity of anti-*GLIS2* *in vivo* by colocalization to primary cilia of GFP-tagged *GLIS2* transfected into HEK293T cells with the anti-*GLIS2* antibody P100 (Fig. 2g-i). It is tempting to speculate that cilia localization of *GLIS2* may depend on its zinc fingers, which are highly similar in protein sequence to the zinc fingers of *Gli2* and *Gli3*, which are also known to localize to cilia¹¹.

To gain insight into the physiologic and pathophysiological roles of the *GLIS2* transcription factor, we analyzed mice with a targeted disruption of the *Glis2* gene (Fig. 3a,b). β -galactosidase staining of 8-week-old kidneys from mice carrying one *Glis2^{lacZ}* allele uncovered *Glis2* expression throughout all renal tubule segments at various expression levels but not in glomerular, mesenchymal or endothelial cells (Fig. 3c-h), consistent with the *in situ* expression analysis (data not shown). Staining was enhanced at this time point in the inner stripe of the outer medulla (Fig. 3c,d). *Glis2^{lacZ}* expression was also detected in the epithelial cells of Bowman's capsule (Fig. 3e). Inter-crossing of heterozygous *Glis2^{lacZ/+}* mice resulted in the generation of homozygous *Glis2^{lacZ/lacZ}* mice, which were born in the expected mendelian ratio. At postnatal day 5 (P5), β -galactosidase staining of

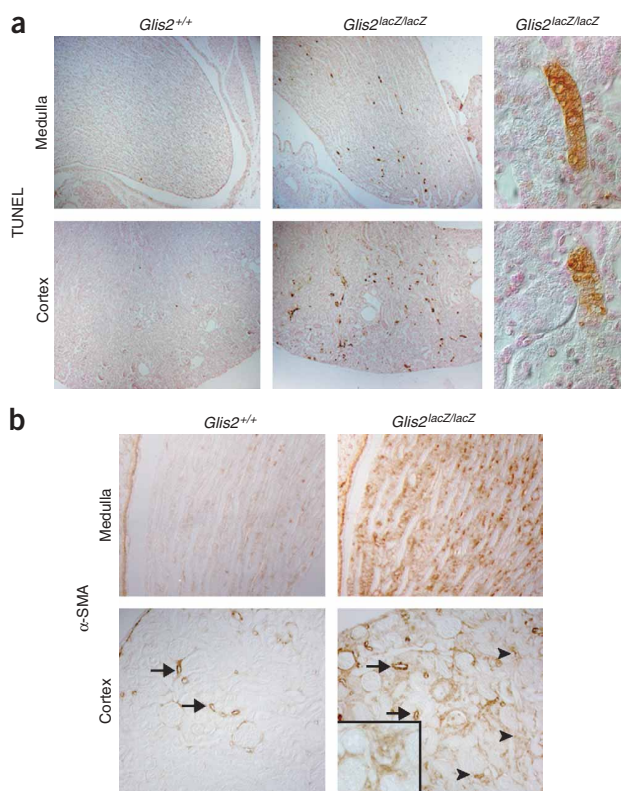


Figure 5 Increased apoptosis and α -smooth muscle actin expression in *Glis2^{lacZ/lacZ}* mutant kidneys. **(a)** Apoptotic cells are seen throughout 4-week-old *Glis2^{lacZ/lacZ}* mutant kidneys, as illustrated by TUNEL-positive cells in the inner medulla (upper row) and cortex (lower row), but not in wild-type controls. Higher magnification demonstrates restriction of TUNEL-positive cells to renal tubules. **(b)** Immunohistochemistry with an antibody to α -smooth muscle actin (SMA) uncovers increased expression of α -SMA in the inner medulla (upper row) and cortex around the glomeruli in the cortical region (lower row) in *Glis2^{lacZ/lacZ}* mutant kidneys but not in controls. Arrows mark positive α -SMA staining of blood vessels in wild-type and mutant kidneys. Arrowheads point to clusters of α -SMA-positive cells in the cortical region. Inset shows higher magnification of such a region.

Severe atrophy was the most notable pathogenic feature of the renal phenotype in *Glis2^{lacZ/lacZ}* mutant mice. Therefore, we performed a TUNEL assay to test for apoptosis. At 4 weeks after birth, significant apoptosis was apparent throughout the renal tubules in homozygous *Glis2^{lacZ/lacZ}* mice but not in wild-type littermates. Careful examination of the apoptotic cells showed that only cells within the renal tubule underwent apoptosis, whereas interstitial and endothelial cells did not (Fig. 5a). At the same time, we did not detect any significant proliferation of renal tubular epithelial cells in either *Glis2^{lacZ/lacZ}* mutant or control kidneys, according to phospho-histone H3 staining (data not shown). Interstitial collagen-producing cells, also referred to as myofibroblasts, express α -smooth muscle actin (α -SMA) and have been shown to be increased in number in fibrotic tissue^{12,13}. Consistent with the overall phenotypic appearance, at 4 weeks after birth we observed an already strong increase in α -SMA-positive cells in the medulla and cortex region of *Glis2^{lacZ/lacZ}* mutant kidneys, compared with control kidneys (Fig. 5b).

One of the persistent challenges in understanding the pathogenesis of cystic kidney 'ciliopathies' is the paradox that in polycystic kidney disease there is kidney enlargement, whereas in NPHP there is progressive reduction of organ size⁶. Therefore, we performed expression profiling of kidneys using the GE/Codelink system, comparing wild-type and homozygous *Glis2^{lacZ/lacZ}* mice at 4 weeks of age. We chose this time point because at this stage, kidneys are fully matured, and there were no recognizable size differences between wild-type and *Glis2^{lacZ/lacZ}* mutant kidneys (Fig. 4a). We decided *a priori* to consider only genes with greater than twofold significant differences in expression. By this criterion, a total of 552 probes were differentially expressed between wild-type and *Glis2^{lacZ/lacZ}* mutant mice (a full list of genes is given in Supplementary Table 1 online), nearly all genes fulfilling this criterion were upregulated in the absence of *Glis2*, consistent with the proposed role of *Glis2* as a transcriptional repressor⁹. To identify possible direct targets of *Glis2*, we searched for Gli consensus binding sites in the promoter proximity of these up-regulated genes (Supplementary Fig. 3a online), realizing that *Gli1*, a target of the hedgehog pathway, is upregulated in *Glis2^{lacZ/lacZ}* mutant kidneys (Fig. 6). It is well established that *Gli1* gene transcription is regulated through Gli binding sites in its promoter¹⁴. Transient transfection assays demonstrated that *Glis2* can indeed suppress *Gli1*-dependent transcriptional activation from consensus Gli binding site-containing luciferase reporter constructs (Supplementary Fig. 3b online). Notably, genes that have been found to be upregulated in *Gli1* overexpression studies, such as *Snail* (also known as *Snail1*) (ref. 15), were also upregulated in *Glis2^{lacZ/lacZ}* mutant kidneys (Fig. 6a), whereas other known renal Gli targets like *Bmp4*, *Pax2*, *Sall1*, *Cnd1* (cyclin D1) or *Mycn* (*N-myc*) were not (data not shown)¹⁶. Thus, we propose a model known as a 'feed-forward repression' strategy¹⁷, in which *Glis2* suppresses not only *Gli1*

kidneys from *Glis2^{lacZ/lacZ}* mutant mice did not uncover any obvious developmental abnormalities (Fig. 3i), with similar numbers of glomeruli present in both genotypes (data not shown). Similarly, gene chip expression profiling comparing P5 wild-type and mutant kidneys did not yield any significant differences between the wild-type and *Glis2^{lacZ/lacZ}* mutant mice at this early stage (data not shown). This demonstrates that until this stage, loss of *Glis2* seems to have no major consequences. From 4 weeks to 6 months, kidneys from *Glis2^{lacZ/lacZ}* mutant mice substantially decreased in size and weight, in contrast to wild-type control littermates (weight: 0.14 g versus 0.22 g; volume: 120 μ l versus 180 μ l; $n = 6$; $P < 0.05$). Periodic Acid Schiff's (PAS) staining performed on *Glis2^{lacZ/lacZ}* mutant kidney sections at various time points after birth demonstrated that cortex, inner medulla and outer medulla were becoming progressively atrophic over the course of 8 weeks to 6 months (Fig. 4a). The characteristic hallmark of NPHP, loss of corticomedullary differentiation, was appreciable at 4 weeks and pronounced at 8 weeks (Fig. 4a). Trichrome-Masson staining of *Glis2^{lacZ/lacZ}* mutant kidneys demonstrated that at 8 weeks, the hallmarks of NPHP were already present and were very pronounced at 6 months⁶. First, there was diffuse tubulointerstitial cell infiltration with interstitial fibrosis and deposition of collagen throughout the kidney. Second, there was tubular basement membrane disintegration with tubular atrophy and cysts, which was markedly similar to the findings in human NPHP. In addition, we also noted glomerular cysts (Fig. 4b,c). Examination of other organs such as the nervous system or somites, where *Glis2* expression is observed during development, did not uncover any gross histological changes consistent with the absence of any obvious motor coordination or behavioral abnormalities (data not shown). These observations suggest that, similar to the situation in the embryonic kidney, compensation by other *Glis* family members may occur.

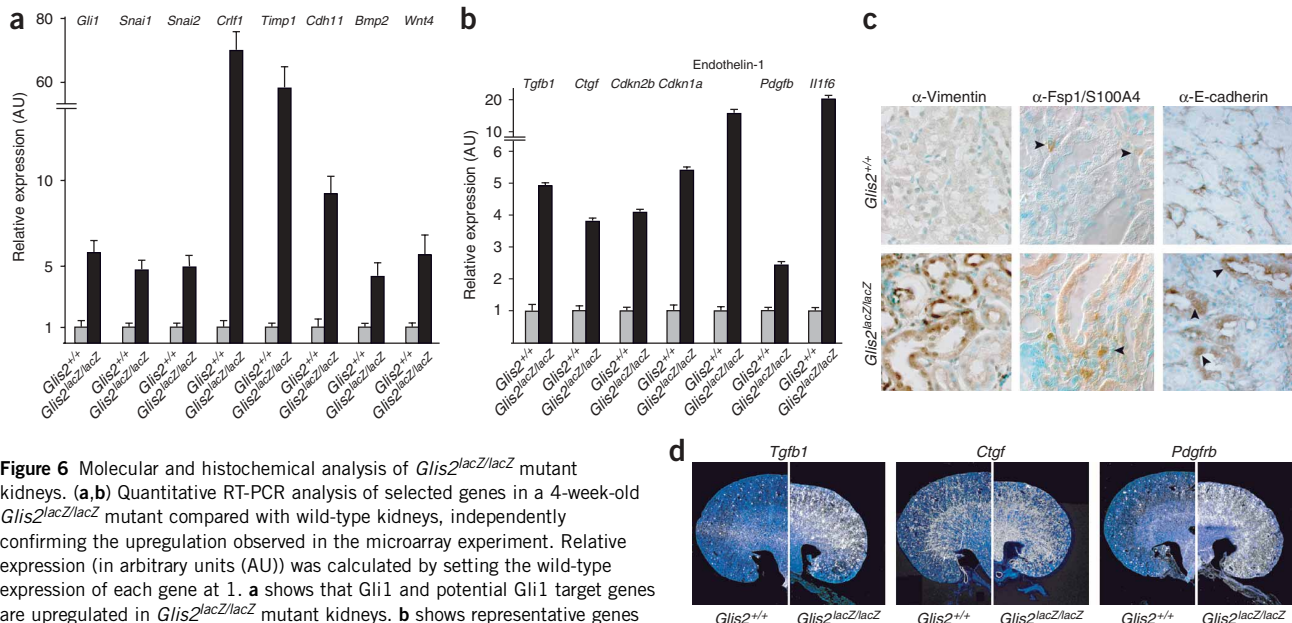


Figure 6 Molecular and histochemical analysis of *Glis2^{lacZ/lacZ}* mutant kidneys. (**a,b**) Quantitative RT-PCR analysis of selected genes in a 4-week-old *Glis2^{lacZ/lacZ}* mutant compared with wild-type kidneys, independently confirming the upregulation observed in the microarray experiment. Relative expression (in arbitrary units (AU)) was calculated by setting the wild-type expression of each gene at 1. **a** shows that *Glil* and potential *Glil* target genes are upregulated in *Glis2^{lacZ/lacZ}* mutant kidneys. **b** shows representative genes involved in epithelial to mesenchymal transition (EMT), genes regulated by *Tgfb1* and genes involved in fibrosis and apoptosis. Error bars represent s.e.m. ($P < 0.05$ for all samples). (**c**) Immunohistochemistry for vimentin, Fsp1/S100A4 and E-cadherin. Renal tubules in *Glis2^{lacZ/lacZ}* mutant but not control kidneys stain positive for vimentin. In *Glis2^{lacZ/lacZ}* mutant kidneys, Fsp1/S100A4-positive renal tubule cells are seen, as well as positive interstitial cell clusters between the tubules (arrowhead). In contrast, only sparsely distributed Fsp1/S100A4-positive cells are seen in control kidneys (arrowheads). Cytosolic redistribution of E-cadherin is observed in a subset of *Glis2^{lacZ/lacZ}* mutant renal tubules (arrowhead), which is never observed in wild-type kidneys. (**d**) *In situ* hybridization analysis for *Tgfb1*, *Ctgf* and *Pdgfrb* in 5-week-old wild type and *Glis2^{lacZ/lacZ}* mutant kidneys. Note size reduction and increased mRNA expression (white signal) in mutant kidneys.

transcription but, in addition, suppresses a *Glil*-activated transcription factor to maintain homeostasis in the adult kidney (Supplementary Fig. 3c online).

It has been proposed that most of the fibroblast-like cells seen in tubulointerstitial cell infiltration arise by epithelial-to-mesenchymal transition (EMT) of renal tubular cells to escape apoptosis^{13,18}. The upregulation of *Snai1* and *Snai2* (also known as *Snail* and *slug* (Fig. 6a)), which can drive EMT by themselves¹⁹, as well as the EMT-associated markers Fsp-1 (also known as S100A4) and vimentin (Vim) detected in *Glis2^{lacZ/lacZ}* mutant kidneys (Supplementary Fig. 3d), prompted us to test if EMT is active in our mouse model. Consistent with the observed tubulointerstitial cell infiltration, we observed many Fsp1-positive cells between renal tubules of *Glis2^{lacZ/lacZ}* mutant kidneys (Fig. 6c). In addition, a significant proportion of renal tubules stained positive for the EMT-specific markers Fsp1 and vimentin in *Glis2^{lacZ/lacZ}* mutant kidneys, suggesting that these tubular cells were about to undergo EMT (Fig. 6c). A crucial step in EMT is loss of epithelial polarity. Basolateral staining of E-cadherin is correlated with the structural identity and polarity of renal tubular epithelial cells. Staining for E-cadherin in *Glis2^{lacZ/lacZ}* mutant kidneys showed that it was redistributed from the basolateral membrane to the cytoplasm in a subset of renal tubules (Fig. 6c), suggesting the loss of cell polarity in these tubular epithelial cells.

Besides the putative *Glis2*- and *Glil*-regulated genes, we grouped additional differentially expressed genes according to biological meaning using GO-GETTER software (Supplementary Fig. 4 online). Representative transcripts overexpressed in *Glis2^{lacZ/lacZ}* mutant kidneys within groups relevant to biological processes of the observed kidney phenotype are shown in Figure 6b and Supplementary Figure 3d. Group 1 comprised known markers of EMT²⁰, group

2 comprised genes regulated by transforming growth factor beta 1 (TGF β -1)²¹, group 3 consisted of cytokines and chemokines²² and group 4 consisted of markers of fibrosis and apoptosis²⁰. Consistent with the prominence of tubulointerstitial fibrosis in NPHP⁶, genes implicated in promoting fibrosis were upregulated, most prominently TGF β -1 and connective tissue growth factor (CTGF), a positive modulator of TGF β signaling²³ (Fig. 6b,d). Both genes have been implicated in interstitial fibrosis and EMT. In agreement with the strong expression of TGF β -1 throughout the mutant kidney, TGF β -1 target genes²¹, including the two cell-cycle inhibitors *Cdkn1a* (p21) and *Cdkn2b* (p15), were upregulated (Fig. 6b), consistent with the absence of increased proliferation in renal tubular epithelial cells of *Glis2^{lacZ/lacZ}* mutant kidneys. In addition, other factors implicated in EMT and promotion of renal fibrosis were upregulated. These included endothelin-1 (*Edn1*), *Pdgfrb* (ref. 24) and its receptor *Pdgfrb*, a marker for renal fibroblasts²⁵ (Fig. 6b,d). These also included *Il1f6*, a member of the interleukin-1 family (Fig. 6b)²⁶. Notably, expression of *Tgfb1* and *Pdgfrb* was strongest at the corticomedullary border (Fig. 6d). This is the same region where *Glis2* expression was strongest (Fig. 3c), where *Glis2^{lacZ/lacZ}* mutant kidneys underwent the strongest atrophy (Fig. 4a), and where tubular atrophy is most pronounced in NPHP⁶.

By presenting evidence for EMT and increased apoptosis in the absence of proliferation in *Glis2^{lacZ/lacZ}* mutant renal tubular cells, we here provide data that may explain progressive fibrosis and loss of kidney size in nephronophthisis, which is in contrast to the increase in kidney size seen in other renal cystic 'ciliopathies' such as polycystic kidney disease¹². *GLIS2* and *Glis2* belong to the Kruppel-like C2H2 zinc finger protein subfamily, which includes the *Drosophila melanogaster* ortholog *Cubitus interruptus* (*Ci*) and the mammalian

transcription factors of the GLI, ZIC, and GLIS families⁸. The hedgehog signaling pathway and the Gli proteins are essential during murine kidney development^{16,27}. Furthermore, elevated hedgehog pathway activity has been demonstrated to contribute to EMT in some tumor types²⁸. In this respect, it is noteworthy that all three Glis family members are expressed in overlapping patterns in the adult mouse kidney (data not shown), suggesting redundancy, which may explain the more severe pathology at the corticomedullary border in *Glis2^{lacZ/lacZ}* mutant mice. Notably, recessive mutations of *GLIS3* have recently been shown to cause polycystic kidneys in a syndrome of neonatal diabetes mellitus, with congenital hypothyroidism (OMIM #610199)²⁹. In this way, the function of Glis proteins, such as Glis2, may link cystic kidney disease due to mutations in genes encoding members of the hedgehog signaling pathway (such as *wim* and *fxo*) with renal cystic diseases caused by mutations in genes encoding proteins of primary cilia (for example, NPHP1–NPHP6)^{11,30}. We propose that whereas the hedgehog pathway is active in mesenchymal to epithelial transition in renal tubulogenesis²⁷, loss of function of downstream effectors of hedgehog signaling may lead to the reverse process (EMT) and thereby to the NPHP phenotype. In summary, by demonstrating an NPHP phenotype in humans and mice upon loss of function of Glis2, we show that human and mouse Glis2 are required for the maintenance of normal kidney tissue architecture and function through prevention of apoptosis and fibrosis.

METHODS

Subjects. We obtained blood samples and pedigrees after obtaining informed consent from individuals with NPHP and/or their parents. Experiments on humans were approved by the University of Michigan Institutional Review Board. The diagnosis of NPHP was based on the following criteria: (i) the clinical course and renal ultrasound or renal biopsies were compatible with the diagnosis of NPHP as judged by a (pediatric) nephrologist, and (ii) patients had entered end-stage renal disease.

Linkage analysis. We performed a genome-wide search for linkage in 25 consanguineous kindred with NPHP using the GeneChip Human Mapping 10K 2.0 Xba Array from Affymetrix. Homozygous regions were identified on the basis of nonparametric linkage statistics (NPL) and were plotted graphically across the human genome using Gnu Plot (<http://www.gnu.org>). Homozygous regions were further genotyped using highly polymorphic microsatellite markers in order to confirm or exclude homozygosity.

Mutational analysis. Mutational analysis was performed by PCR and direct sequencing using exon-flanking primers to human *GLIS2* (Supplementary Table 2 online). We screened 470 individuals with NPHP and 94 healthy controls for mutations in *GLIS2* using heteroduplex mismatch-specific *CelI* DNA endonuclease digestion. An equal amount of PCR product from both the screening panel and healthy control samples were mixed and subjected to cycles of denaturation and annealing. Aliquots of the mix were digested using mismatch-specific DNA Surveyor endonuclease (Transgenomic) for 5 min at 37 °C, and the reaction was stopped by adding 0.15 M EDTA. Electrophoresis on a 1.5% agarose gel was performed, and samples with sequence variants were selected by the presence of aberrant DNA bands resulting from *CelI* DNA endonuclease digest and were then subjected to direct exon sequencing.

Cell culture and immunofluorescence. MDCK-II and HEK293T cells were obtained from ATCC and were cultured as recommended. Cells were grown on cover slips in DMEM (Gibco) supplemented with 10% FBS (Atlanta Biologicals) in the presence of penicillin G (10 units ml⁻¹), streptomycin sulfate (10 µg ml⁻¹) and amphotericin B (0.25 µg ml⁻¹) (Gibco). At confluence, cells were washed in 1 × PBS, fixed with 4% formaldehyde for 15 min, permeabilized with 0.1% Triton for 5 min and blocked with 2% goat serum (Abcam) for 2 h. After immunostaining, cover slips were mounted using ProLong antifade with DAPI (Molecular Probes). Confocal laser microscopy was performed using a Zeiss

LSM 510 confocal microscope mounted on a Zeiss Axiovert 100M inverted microscope (Zeiss). Images were acquired using a 63 × Plan Neofluor water-immersion objective (Zeiss). Images were edited using Adobe Photoshop 7.0. Transfections of HEK293T were conducted using FUGENE 6 (Roche Diagnostics) at cell confluence. The expression of recombinant protein was assessed after 36 h. Polyclonal antibody P100 against GLIS2 was purchased from Aviva Systems Biology (Aviva Systems Biology). An antibody against acetylated α -tubulin was obtained from Sigma. Fluorescently labeled Alexa-Fluor secondary antibodies were obtained from Molecular Probes. All antibodies were used at the concentrations suggested by the manufacturer. Negative controls for the secondary antibodies used are available from the authors on request.

***Glis2^{lacZ}* targeting vector.** Three overlapping *Glis2*-positive BAC clones were isolated from a 129-mouse BAC library (Invitrogen/Research Genetics). A 7.5-kb genomic *HindIII* fragment containing coding exons 3, 4 and 5 of *Glis2* was cloned into pBluescript. The targeting vector contains a 4-kb 5'-homologous region (*Asp718-NotI* fragment) and a 3 kb 3'-homologous region (*NotI* fragment). Both homologous regions were amplified by PCR from the *HindIII* genomic clone, and the *Asp718* and *NotI* restriction sites were included in the primer sequences (Supplementary Table 2). The coding region (amino acids 127–247) was replaced with an in-frame fused *nlslacZ* cassette followed by the self-excisable *neo^r* cassette (ACN). For negative selection, a *MCI-DTA* cassette was placed at the end of the 3'-homologous region.

Generation of *Glis2^{lacZ}* mutant allele. Standard embryonic stem cell technology using an E14.1 embryonic stem cell line was employed. The resulting male chimeras were mated with C57Bl/6J females, and agouti offspring were genotyped by PCR (for primer sequences, see Supplementary Table 2). Analyses was performed with *Glis2^{lacZ}* mice, which were backcrossed for ten generations on a C57Bl/6J background. Mice were housed in specific pathogen-free controlled conditions. Food and water were available *ad libitum*. The procedures for performing animal experiments were in accordance with the principles and guidelines of the LAR/European Molecular Biology Laboratory (EMBL).

Histology and immunohistochemistry. Kidney expression of the *lacZ* reporter gene present in the replacement vectors for the *Glis2* gene was visualized by staining frozen tissue sections for β -galactosidase activity. We used a β -galactosidase staining solution containing Bluo-Gal substrate (20 mM K₃Fe(CN)₆; 20 mM K₄Fe(CN)₆·3H₂O; 0.01% sodium deoxycholate; 2 mM MgCl₂; 0.02% (vol/vol) NP-40; 1 mg ml⁻¹ Bluo-Gal). PAS staining of kidney sections were performed with Gill's hematoxylin #3 (Polysciences), followed by dehydration in an ascending ethanol series, followed by a xylene treatment for clearance and mounting. Kidneys for TUNEL assays were fixed in 4% paraformaldehyde (PFA) for 30 min and were assayed according to the manufacturer's instructions (Apoptag, Chemicon). For immunohistochemistry, kidneys were fixed in 2% PFA at 4 °C overnight. We hydrated 7-µm-thick paraffin sections and blocked nonspecific binding in 5% serum, corresponding to the secondary antibody in 1 × TBS with 4% Triton X-100. For antibodies to E-cadherin (Sigma, monoclonal mouse, 1:1,000) and smooth muscle actin (Sigma, monoclonal mouse, 1:1,000), endogenous peroxidase was inactivated using 10% methanol plus 3% hydrogen-peroxide in PBS, before blocking with 5% serum. Staining for S100A4 (Abcam, polyclonal anti-rabbit, 1:50) and vimentin (Abcam, polyclonal anti-rabbit, 1:100) required an antigen retrieval method. Slides were incubated along with primary antibodies overnight at 4 °C and washed in 1 × TBS with 4% Triton X-100 twice; secondary biotinylated antibodies to mouse or rabbit (Vector) were incubated for 1 h at room temperature and developed with the 5-diaminobenzidine (DAB) substrate kit (Vector). Counterstaining was done using methyl green.

In situ hybridization analysis. Tissues were fixed in 10% formalin. Hybridization with ³⁵S-labeled antisense RNA probes was done as previously described on 20-µm cryosections. Hybridization signals were detected by autoradiography; slides were subsequently immersed in photo emulsion (KODAK) and developed.

RNA isolation. Kidneys from 4-week-old wild-type and *Glis2^{lacZ/lacZ}* mutant mice were excised from the animal after perfusion with PBS, snap-frozen in liquid nitrogen and stored at -80°C . For each microarray, kidney RNA was isolated using the RNeasy Mini Kit (Qiagen), following the manufacturer's instructions. Briefly, frozen kidneys were homogenized in buffer RLT using a mortar and pestle, followed by a syringe and needle. The optional on-column DNase digestion was performed according to standard protocols (Qiagen). The RNA concentration was determined by ultraviolet spectrophotometry, and RNA integrity was analyzed by agarose gel electrophoresis.

Microarray hybridization and feature extraction. For microarray target preparation and hybridization, 2 μg of total RNA from whole kidney were used according to the manufacturer's instructions. Three biological replicates were processed for each genotype. In brief, the Codelink Expression Assay Reagent Kit (GE Healthcare) was used for cDNA synthesis and *in vitro* transcription, and the cDNA was purified using a PCR purification kit (Qiagen). The biotinylated cRNA (Biotin-16-UTP, Roche) was recovered using the RNeasy kit. The cRNA was quantified with an ultraviolet spectrophotometer, and 10 μg cRNA was fragmented and hybridized to Codelink Mouse Whole-Genome Bioarrays (GE Healthcare). After incubation at 37°C for 18 h, the arrays were washed, stained with Streptavidin-Cy5 (GE Healthcare) and scanned using a GenePix scanner (Axon Instruments) as described in the manufacturer's manual. The scanned image files were analyzed using the Codelink Expression Analysis v4.0 software.

Microarray data analysis and real-time PCR. We analyzed the data obtained from the Codelink software package using GeneSpring (Agilent Technologies). Values below 0.01 were set to the cutoff of 0.01. Data were normalized per chip (each array was normalized to the 50th percentile of the measurements for that array) and per gene (each gene was divided by the median of its measurement in all samples). To determine differential expression, we averaged the triplicate samples. Only genes showing a present flag ('P') in at least three out of six samples and showing a minimum difference in expression of greater than twofold were included in the analysis. Statistical significance was calculated by a *t* test with a *P* value of <0.05 (with no multiple testing correction). Quantitative SYBR Green quantitative RT-PCR on an ABI 7500 system was performed on RNA extracted from whole kidneys of the respective genotype using the primers shown in **Supplementary Table 2**. Data analysis was done using a relative expression software tool (REST) using *Gapdh* and 18S as the reference genes.

Accession codes. The data discussed in this publication have been deposited in NCBI's Gene Expression Omnibus (GEO) and are accessible through GEO Series accession number GSE6113.

Note: Supplementary information is available on the Nature Genetics website.

ACKNOWLEDGMENTS

We thank the EMBL/Heidelberg Transgenic Facility for generation of chimeric animals and the staff of the EMBL Laboratory Animal Resources for expert animal husbandry. The US National Institutes of Health supported F.H. (DK064614, DK068306, DK069274) and J.O.T. (DK071108); F.H. is the Frederick G.L. Huetwell Professor and Doris Duke Distinguished Clinical Scientist. This research was further supported by the German Federal Ministry of Science and Education through the National Genome Research Network (D.S., G.N., C.B. and P.N.) and the Fritz-Thyssen Stiftung (Germany) (M.T.).

AUTHOR CONTRIBUTIONS

M.A. carried out positional cloning, mutation analysis, immunofluorescence studies, minigene expression studies and clinical evaluation. N.H.U. performed gene expression analysis, transient transfections and overall characterization of *Glis2* mutant mice. V.H.S. and K.A. generated *Glis2* mutant mice. J.F.O.T. carried out positional cloning and fine mapping. E.O. carried out the genome-wide search for linkage. C.K. and A.-C.T. performed histological analysis. J.H. carried out exon sequencing of a large number of NPHP patients and healthy control individuals. J.A.S. was involved in the genome-wide search for linkage and positional cloning. D.S. and G.N. carried out statistical evaluation of the genome-wide search for linkage. C.B. and P.N. performed SNP chip analysis for the genome-wide search for linkage. A.E.C. was involved in clinical characterization of subjects. F.H. designed the study on gene identification in individuals with NPHP and directed all studies on the genome-wide search for linkage, positional

cloning, mutation analysis, immunofluorescence, minigene expression studies and clinical evaluation. M.T. initiated the project and designed, directed and analyzed all animal studies. F.H. and M.T. wrote the paper, with feedback from the other authors.

COMPETING INTERESTS STATEMENT

The authors declare no competing financial interests.

Published online at <http://www.nature.com/naturegenetics>

Reprints and permissions information is available online at <http://npg.nature.com/reprintsandpermissions>

- Hildebrandt, F. *et al.* A novel gene encoding an SH3 domain protein is mutated in nephronophthisis type 1. *Nat. Genet.* **17**, 149–153 (1997).
- Otto, E.A. *et al.* Mutations in *INVS* encoding inversin cause nephronophthisis type 2, linking renal cystic disease to the function of primary cilia and left-right axis determination. *Nat. Genet.* **34**, 413–420 (2003).
- Hildebrandt, F. & Otto, E. Cilia and centrosomes: a unifying pathogenic concept for cystic kidney disease? *Nat. Rev. Genet.* **6**, 928–940 (2005).
- Sayer, J.A. *et al.* The centrosomal protein nephrocystin-6 is mutated in Joubert syndrome and activates transcription factor ATF4. *Nat. Genet.* **38**, 674–681 (2006).
- Watnick, T. & Germino, G. From cilia to cyst. *Nat. Genet.* **34**, 355–356 (2003).
- Zollinger, H.U. *et al.* Nephronophthisis (medullary cystic disease of the kidney). A study using electron microscopy, immunofluorescence, and a review of the morphological findings. *Helv. Paediatr. Acta* **35**, 509–530 (1980).
- Igarashi, P. & Somlo, S. Genetics and pathogenesis of polycystic kidney disease. *J. Am. Soc. Nephrol.* **13**, 2384–2398 (2002).
- Zhang, F. & Jetten, A.M. Genomic structure of the gene encoding the human GLI-related, Kruppel-like zinc finger protein GLIS2. *Gene* **280**, 49–57 (2001).
- Zhang, F. *et al.* Characterization of *Glis2*, a novel gene encoding a Gli-related, Kruppel-like transcription factor with transactivating and repressor functions. Roles in kidney development and neurogenesis. *J. Biol. Chem.* **277**, 10139–10149 (2002).
- Mollet, G. *et al.* Characterization of the nephrocystin/nephrocystin-4 complex and subcellular localization of nephrocystin-4 to primary cilia and centrosomes. *Hum. Mol. Genet.* **14**, 645–656 (2005).
- Haycraft, C.J. *et al.* Gli2 and Gli3 localize to cilia and require the intraflagellar transport protein polaris for processing and function. *PLoS Genet* **1**, e53 (2005).
- Okada, H. *et al.* Progressive renal fibrosis in murine polycystic kidney disease: an immunohistochemical observation. *Kidney Int.* **58**, 587–597 (2000).
- Lin, F., Moran, A. & Igarashi, P. Intrarenal cells, not bone marrow-derived cells, are the major source for regeneration in postischemic kidney. *J. Clin. Invest.* **115**, 1756–1764 (2005).
- Dai, P. *et al.* Sonic Hedgehog-induced activation of the Gli1 promoter is mediated by Gli3. *J. Biol. Chem.* **274**, 8143–8152 (1999).
- Louro, I.D. *et al.* Comparative gene expression profile analysis of Gli1 and c-MYC in an epithelial model of malignant transformation. *Cancer Res.* **62**, 5867–5873 (2002).
- Hu, M.C. *et al.* GLI3-dependent transcriptional repression of Gli1, Gli2 and kidney patterning genes disrupts renal morphogenesis. *Development* **133**, 569–578 (2006).
- Mangan, S. & Alon, U. Structure and function of the feed-forward loop network motif. *Proc. Natl. Acad. Sci. USA* **100**, 11980–11985 (2003).
- Strutz, F. & Muller, G.A. Renal fibrosis and the origin of the renal fibroblast. *Nephrol. Dial. Transplant.* **21**, 3368–3370 (2006).
- Moreno-Bueno, G. *et al.* Genetic profiling of epithelial cells expressing e-cadherin repressors reveals a distinct role for snail, slug, and e47 factors in epithelial-mesenchymal transition. *Cancer Res.* **66**, 9543–9556 (2006).
- Harris, R.C. & Neilson, E.G. Toward a unified theory of renal progression. *Annu. Rev. Med.* **57**, 365–380 (2006).
- Shi, Y. & Massague, J. Mechanisms of TGF-beta signaling from cell membrane to the nucleus. *Cell* **113**, 685–700 (2003).
- Anders, H.J., Vielhauer, V. & Schlondorff, D. Chemokines and chemokine receptors are involved in the resolution or progression of renal disease. *Kidney Int.* **63**, 401–415 (2003).
- Abreu, J.G., Ketpura, N.I., Reversade, B. & De Robertis, E.M. Connective-tissue growth factor (CTGF) modulates cell signalling by BMP and TGF-beta. *Nat. Cell Biol.* **4**, 599–604 (2002).
- Bonner, J.C. Regulation of PDGF and its receptors in fibrotic diseases. *Cytokine Growth Factor Rev.* **15**, 255–273 (2004).
- Qi, W. *et al.* Integrated actions of transforming growth factor-beta1 and connective tissue growth factor in renal fibrosis. *Am. J. Physiol. Renal Physiol.* **288**, F800–F809 (2005).
- Zhang, M., Tang, J. & Li, X. Interleukin-1beta-induced transdifferentiation of renal proximal tubular cells is mediated by activation of JNK and p38 MAPK. *Nephron Exp. Nephrol.* **99**, e68–e76 (2005).
- Yu, J., Carroll, T.J. & McMahon, A.P. Sonic hedgehog regulates proliferation and differentiation of mesenchymal cells in the mouse metanephric kidney. *Development* **129**, 5301–5312 (2002).
- Huber, M.A., Kraut, N. & Beug, H. Molecular requirements for epithelial-mesenchymal transition during tumor progression. *Curr. Opin. Cell Biol.* **17**, 548–558 (2005).
- Senee, V. *et al.* Mutations in GLIS3 are responsible for a rare syndrome with neonatal diabetes mellitus and congenital hypothyroidism. *Nat. Genet.* **38**, 682–687 (2006).
- Huangfu, D. *et al.* Hedgehog signalling in the mouse requires intraflagellar transport proteins. *Nature* **426**, 83–87 (2003).